Macromolecules
ARTICLE

Macromolecules **2009**, *42*, 6741–6747 **6741**
DOI: 10.1021/ma901182u

Effects of Layer Thickness and Annealing of PEDOT:PSS Layers in Organic Photodetectors

Bettina Friedel,* Panagiotis E. Keivanidis, Thomas J. K. Brenner, Agnese Abrusci, Christopher R. McNeill, Richard H. Friend, and Neil C. Greenham

Cavendish Laboratory, Department of Physics, University of Cambridge, J. J. Thomson Avenue, Cambridge CB3 0HE, United Kingdom

Received June 2, 2009; Revised Manuscript Received July 17, 2009

ABSTRACT: We have investigated the effects of thickness variation and thermal treatment of the electrode polymer poly(3,4-ethylenedioxythiophene):poly(styrenesulfonic acid) (PEDOT:PSS) in photovoltaic and photodetector devices using conjugated polymer blends as the photoactive material. By variation of the PEDOT:PSS layer thickness between 25 and 150 nm, we found optimum device performance, in particular low dark current and high external quantum efficiency (EQE) and open-circuit voltage (V_{oc}), at around 70 nm. This has been observed for two different active layers. Annealing studies on the PEDOT:PSS films, with temperatures varied between 120 and 400 °C, showed an optimum device performance, in particular EQE and V_{oc} at 250 °C. This optimum performance was found to be associated with loss of water from the PSS shell of the PEDOT:PSS grains. For annealing temperatures above 260 °C, device performance was dramatically reduced. This was associated with chemical decomposition leading to loss of sulfonic acid, although this did not significantly affect the in-plane conductivity.

Introduction

Poly(3,4-ethylenedioxythiophene) or PEDOT is a conjugated polymer which is widely used in organic optoelectronics. In its doped state, its high conductivity (up to several hundred S cm^{-1}), good optical transparency in thin films, and its high stability make it highly attractive as an electrode material, for example, in light-emitting diodes or photodetectors. In its pure form, PEDOT is not soluble in common solvents and is infusible at reasonable temperatures.[1−3] This problem has been solved by polymerization of PEDOT in the presence of the water-soluble poly (styrenesulfonic acid) (PSS), working as a charge-balancing dopant, forming colloidal particles.[4,5] These are reported to be built from a random coil entanglement of PSS chains with attached PEDOT oligomers, forming particles which consist of a PEDOT-rich core covered by a PSS-rich shell.[4,6−8] These aqueous colloidal solutions are commercially available with different conductivities, since resistivity of the final film can be easily adjusted, as required, by controlling the amount of excess PSS in the solution.[6,7,9] In this way PEDOT:PSS can be easily deposited as thin films via common methods, e.g., spin-casting or inkjet printing. In many types of optoelectronic devices, layers of PEDOT:PSS are sandwiched between the indium−tin oxide (ITO) electrode and the active organic layer. In this role, it fulfills a number of functions: it provides a well-defined work function which is higher than that of ITO, it smoothes the rough ITO surface and so avoids shorts, and it protects the active layer from ingress of indium or oxygen, leading to longer device lifetimes.[8,10−12] Unfortunately, the special nature of this material brings as well some disadvantages. The PEDOT:PSS colloidal solution is strongly acidic and so has the potential to cause degradation in adjacent layers, if water is not completely removed.[13] The morphology of the colloidal particles is gel-like, and they tend, due to the strongly hygroscopic PSS, to swell or shrink considerably, depending on humidity.[2,6,11] During film formation under certain conditions, excess PSS from the colloidal solution seems to form a closed surface layer, which increases the work function but also considerably decreases the perpendicular conductivity.[2,10] These effects influence the final device performance considerably and therefore have been the focus of extensive research in recent years. A wide range of different approaches have been carried out to deal with these problems. One of the most prominent methods is the introduction of secondary dopants, additional to PSS, e.g. in the form of polyols or anionic surfactants, changing film-forming properties, water uptake, or work function.[2,11,12] Different kinds of chemical modification include modifying the PEDOT:PSS colloidal solution with surfactants or organic solvents to suppress screening effects or improve wettability.[11] Thermal treatments of PEDOT:PSS films have also been studied, although there is contradictory evidence as to whether these assist or reduce the formation of a PSS-enriched surface layer.[10,11,14] Other reported results include enhancement of PEDOT crystallinity, changes in surface roughness, diffusion of indium into PEDOT:PSS, or rupture of the ionic bonds between PEDOT and PSS due to annealing.[15−18] Nevertheless, fewer efforts have been made to investigate influences of annealing on the PEDOT:PSS complex itself, preheating effects on the colloidal solution, variation of film thickness, and their consequences for device operation.[19] We therefore believe there is considerable scope remaining for improving device properties by adjustment of film thickness and/or annealing.

In this work, we present a collection of interconnected studies on commonly available PEDOT:PSS, exploring general influences of layer thickness or annealing of deposited films on the performance of polymer blend photovoltaic devices. Therefore, some basic properties of the PEDOT:PSS colloid itself have been investigated, such as particle and film forming morphology, electrical conductivity, thermal behavior and optical properties, and also degradation studies of PEDOT:PSS upon annealing. Device performance studies, demonstrating the consequences

*Corresponding author. E-mail: bf245@cam.ac.uk.

Published on Web 07/29/2009

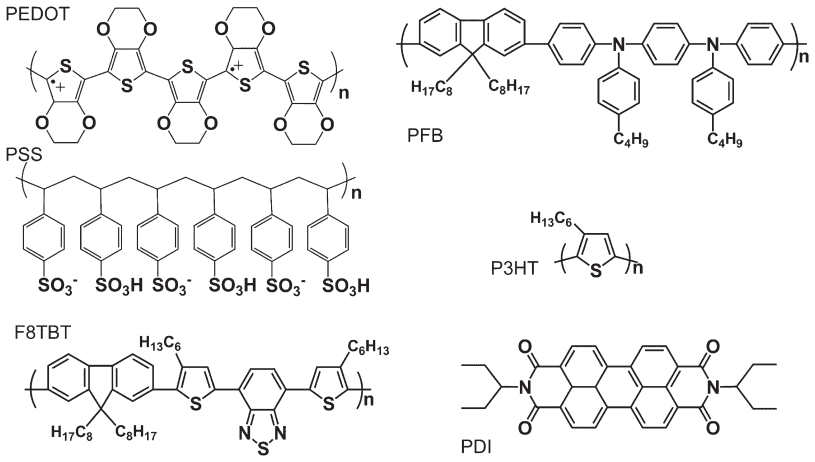

Figure 1. Chemical structures of PEDOT and PSS and structures for the active layer materials F8TBT, PFB, P3HT, and PDI.

arising from specific PEDOT:PSS film properties, have been carried out on devices using two different blend systems as the active layer. Benefits from certain PEDOT:PSS film properties for our photovoltaic devices have in particular been quantified by comparison of external quantum efficiency, dark current, open-circuit voltage, and fill factor.

Experimental Details

1. Materials. All substrates used (glass, ITO glass, silicon) were cleaned by sonication in methanol, acetone, and isopropanol for 20 min each, followed by oxygen plasma etching (250 W, 10 min).

For all experiments a filtered (0.2 μm) aqueous colloidal PEDOT:PSS solution (BaytronP, H.C. Starck GmbH, PSS-enriched by Cambridge Display Technology Ltd.) with a PEDOT-to-PSS ratio of 1:16 has been used. Two different material systems have been used as active layers: polymer/small-molecule blends of poly(9,9-dioctylfluorene-*co*-bis-*N,N*-(4-butylphenyl)-bis-*N,N*-phenyl-1,4 phenylenediamine) (PFB) (Cambridge Display Technology Ltd.) with *N,N′*-bis(1-ethylpropyl)-3,4,9,10-perylene tetracarboxydiimide) (PDI) (Sensient) and all-polymer blends of poly((9,9-dioctylfluorene)-2,7-diyl-*alt*-[4,7-bis(3-hexylthien-5-yl)-2,1,3-benzothiadiazole]-2′,2″-diyl) (F8TBT) (Cambridge Display Technology Ltd.) with poly(3-hexylthiophene) (P3HT) (American Dye Source). Chemical structures for all used materials are displayed in Figure 1. Both blend systems have been studied previously in photodetector or photovoltaic applications. Blends of polyfluorene copolymers like PFB, with the small-molecule PDI, represent a popular model system for processes in general polymer/small-molecule heterojunction devices. EQEs in the order of 20% are obtained, which make this material system attractive for photodetector applications, e.g. in X-ray medical imaging.[20,21] In the case of blends of F8TBT:P3HT, a polyfluorene copolymer with a semicrystalline polythiophene results obtained in solar cells show EQEs up to 26% and power conversion efficiencies of 1.8% under solar simulator conditions, state-of-the-art for all-polymer solar cells. This system benefits from the increased absorption cross section of P3HT:F8TBT blends compared to polymer/fullerene systems and the partially crystalline morphology of P3HT, which can be adjusted e.g. by annealing conditions and has strong influence on charge mobility.[22]

2. Preparation. Generally spin-coating of PEDOT:PSS has been carried out under ambient conditions and any annealing steps or storage under a nitrogen atmosphere. For thickness dependence studies, the spin speed has been varied between 1000 and 7000 rpm, resulting in different films thicknesses from 130 nm down to 25 nm. For all other experiments the spin speed was always adjusted to achieve a final PEDOT:PSS film thickness of 60 nm after any postdeposition treatment steps to ensure comparability. Unless stated otherwise, annealing of the PEDOT:PSS film was performed at 120 °C for 30 min. For annealing studies films have been heated to temperatures between 120 and 400 °C for 30 min. Before measurement or further treatment all the samples have been kept in a nitrogen-filled glovebox to avoid any influence from water or oxygen uptake. Photovoltaic devices have been prepared via the following route. PEDOT:PSS is deposited on a clean ITO−glass substrate and the film post-treated as required (for details, see above). Afterward, the respective photoactive polymer blends are spin-coated on top, with thicknesses of 70 nm for F8TBT:P3HT and 150 nm for PFB:PDI, followed by evaporation of aluminum cathode contacts with a thickness of 100 nm. For the F8TBT:P3HT system a subsequent annealing step is required at 130 °C for 10 min in a N_2 atmosphere. The final devices have an active area of 4.5 mm^2. Finally, they are encapsulated in epoxy resin to avoid environmental influences.

3. Methods. Imaging has been performed using atomic force microscopy (Veeco Dimension 3100 AFM, operated in tapping mode) and high-resolution environmental electron microscopy (FEI Philips XL30 FEG ESEM). Weight and phase changes as a function of temperature have been recorded, using a thermogravimetric analyzer (TA Instruments Q500 TGA) and a differential mechanical analyzer (TA Instruments Q800 DMA). Fourier transform infrared spectroscopy (FTIR) measurements have been made under nitrogen in a benchtop FTIR spectrometer (Nicolet, Nexus 870), using samples prepared on double-side polished silicon wafers. The film thicknesses were measured using a stylus profilometer (Veeco Dektak IIA). Agglomerate size in solution was determined by dynamic light scattering measurements (Malvern Zetasizer). For photophysical characterization, external quantum efficiency (EQE) was measured as a function of wavelength, using a monochromatic light source (100 W tungsten filament lamp, passed through a monochromator) at intensities of around 1 mW/cm^2, with a final spot size smaller than the device active area. The short-circuit current was recorded with a Keithley 237 source-measure unit (SMU). Incident light intensity was continuously monitored during measurement after calibration with a Hamamatsu S8746-01 photodiode. Current−voltage characteristics were recorded in the dark and under illumination using the Keithley 237 SMU. Optical absorbance was recorded with a UV/vis spectrophotometer (HP 8453). Resistance of the PEDOT:PSS films was measured under a nitrogen atmosphere, using a two-point-probe setup on a Karl Suss probe station connected to an HP 4155B semiconductor parameter analyzer. For these measurements, sets of two parallel 50 nm thick gold stripes with a separation of 40 μm have been evaporated on clean glass substrates, followed by deposition of PEDOT:PSS on top and

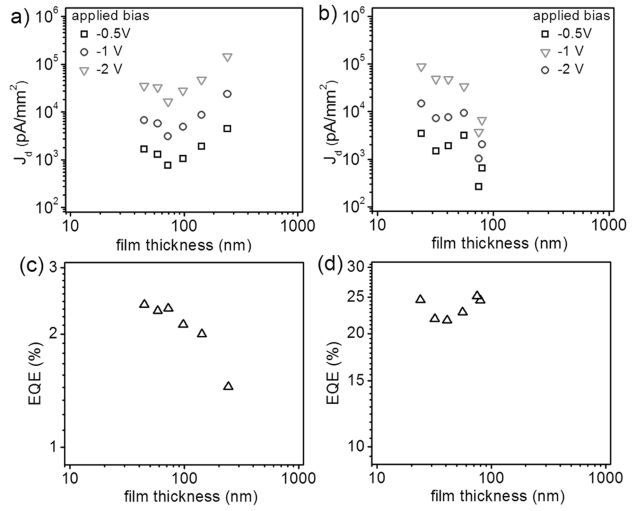

Figure 2. Dark current density vs PEDOT:PSS film thickness in blend devices of (a) PFB:PDI and (b) F8TBT:P3HT. EQE as a function of PEDOT:PSS film thickness for (c) PFB:PDI and (d) F8TBT:P3HT blend devices.

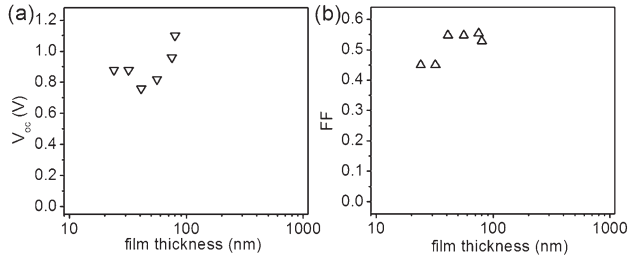

Figure 3. Open-circuit voltage (a) and fill factors (b) for F8TBT:P3HT devices as a function PEDOT:PSS film thickness.

annealing as required. The measurement was performed in-plane by penetrating the polymer to make contact with the gold electrode.

Results and Discussion

1. PEDOT:PSS Thickness Dependence. *Device Performance*. The consequences of different PEDOT:PSS film thickness for the performance of polymer photovoltaic cells, in particular dark current, external quantum efficiency, and current−voltage characteristics under illumination, have been studied. Devices with PEDOT:PSS thickness varying between 25 and 160 nm were compared, keeping the active layer thickness constant. Figure 2a,b shows the dark current densities at different applied reverse bias as a function of thickness. The amount of dark current initially decreases clearly with increasing film thickness, up to a thickness of about 75 nm. When this thickness is exceeded, the dark current density rises again. These results are consistent for both the PFB:PDI and the F8TBT:P3HT devices. The external quantum efficiency for these devices, recorded at 550 nm illumination, is shown in Figure 2c,d. For the PFB:PDI devices the EQE is relatively constant between 20 and 80 nm PEDOT:PSS thickness, with a maximum value at around 75 nm. Further increase of thickness above 80 nm causes the EQE to drop. For F8TBT:P3HT, again the EQE is relatively insensitive to PEDOT:PSS thickness but shows a maximum at 75 nm. The F8TBT:P3HT devices also show a red shift in the photocurrent action spectrum with increasing PEDOT:PSS thickness, characteristic of improved P3HT crystallinity inside the overlying polymer blend.[22] Significant

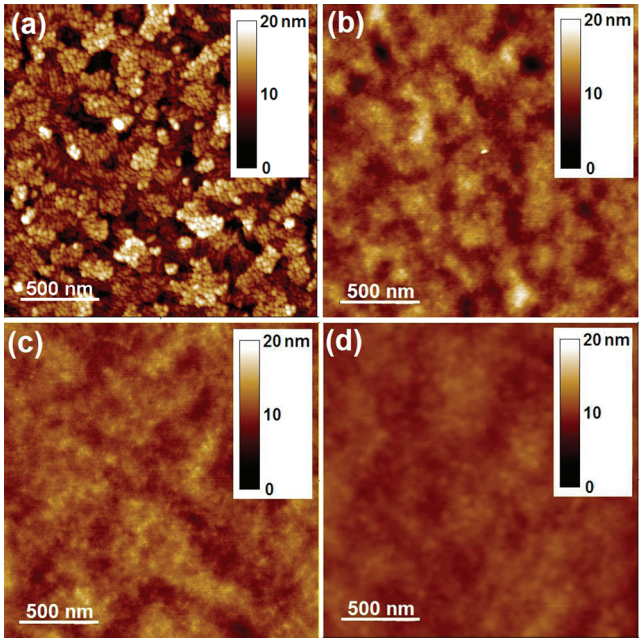

Figure 4. AFM images of (a) bare ITO and of PEDOT:PSS films of thickness (b) 25, (c) 70, and (d) >80 nm (slowly spun).

changes are seen in the open-circuit voltage (V_{oc}) with PEDOT:PSS thickness, as shown in Figure 3a for F8TBT:P3HT devices. V_{oc} stays almost constant for all films up to 60 nm but then increases considerably from 0.8 to 1.1 V. The change in fill factor is shown in Figure 3b, showing improved performance at larger PEDOT:PSS thickness.

PEDOT:PSS Layer Morphology. The morphology of PEDOT:PSS films of different thicknesses on ITO has been investigated. Films of 25−80 nm thickness have been prepared by variation of spinning speed, using the same colloidal PEDOT:PSS solution. Figure 4 shows AFM images of (a) bare ITO and (b−d) films of 25, 70, and >80 nm, respectively. The surface topography gets smoother as the film thickness is increased to 70 nm, with rms roughnesses of 3.5, 1, and 0.7 nm measured for Figure 4a−c, respectively. Interestingly, for the thickest film (Figure 4d), spun at low speed, coarser features appear again, with an rms roughness of 1.2 nm.

We have found that the performance of the photovoltaic cells strongly depends on the thickness of the deposited PEDOT:PSS electrode. These effects may be either direct, due to the change in the properties of the PEDOT:PSS itself, or indirect, due to the influence of the PEDOT:PSS surface properties on the properties of the blend spin-coated on top.

The increased dark currents seen at low PEDOT:PSS thickness are relatively easy to explain based on the changes in surface roughness seen in the AFM. Dark currents may arise when there are low-resistance pathways through the film, and these can be caused by roughness or localized spikes in the topography of the underlying electrode. As shown by the AFM images in Figure 4, adding up to 70 nm of PEDOT:PSS smoothes out features in the underlying ITO substrate, consistent with a reduction in dark current. Further evidence for this hypothesis comes from the observation that a number of devices with very thin PEDOT:PSS were in fact completely short-circuited, consistent with spikes in the ITO.

The increasing dark currents seen for PEDOT:PSS above 70 nm cannot be explained by the influence of the underlying ITO but, interestingly, are also correlated with a higher surface roughness (Figure 4d). We note that for the low spin speeds required to produce thick films the drying dynamics

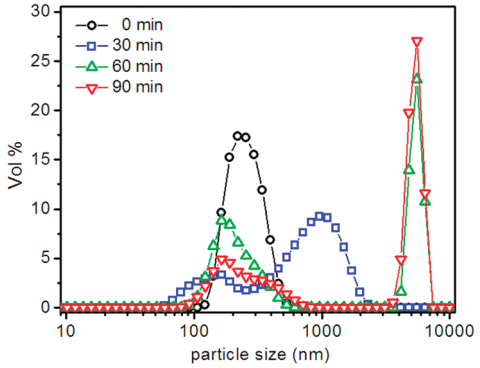

Figure 5. Time evolution of particle/agglomerate size in a sonicated filtered PEDOT:PSS suspension, recorded with dynamic light scattering.

become rather different to those at higher speeds. In particular, a ring of solution is formed at the edge of the substrate due to incomplete centrifugation of the applied solution. The drying of the film becomes significantly slower, and there is some variation in film thickness across the substrate. It is possible that the different drying dynamics are responsible for a change in orientation of the PEDOT grains within the film, which would lead to changes in conductivity and surface properties.[9,23,24] However, our imaging techniques were unable to resolve evidence for this. We do, however, have some information about PEDOT:PSS aggregation which can help to explain the observed increase in surface roughness.

We have performed dynamic light scattering measurements (DLS) on PEDOT:PSS dispersions to study aggregation which may occur during the film drying process. PEDOT:PSS dispersions were ultrasonicated, followed by immediate filtering (0.2 μm) and left to stand before measurement. Particle size distributions were obtained (assuming spherical particles) as shown in Figure 5 for various times after sonication and filtering. The data show a considerable increase in particle/agglomerate size with time. While the as-filtered sample shows just one peak around 200 nm, as expected for the filter size used, after only 30 min a considerable amount of larger particles have been formed, visible as a second peak at around 1 μm. This aggregation with time is likely to occur to some extent during drying of the spin-coated films, at least for the thick films with long drying times. This is consistent with the increased roughness observed in thick films. However, DLS was measured on the PEDOT:PSS particles in swollen state (containing 95% water), while roughness was measured on dried samples, so the final features are smaller.

In addition to the direct effects of the composition and roughness of the PEDOT:PSS surface on device performance, it is worthwhile to consider the indirect effects on the structure of the overlying blend. These effects may be particularly important in explaining the changes seen in EQE and V_{oc}. To study these effects in detail, the photocurrent action spectra of F8TBT:P3HT devices with different PEDOT:PSS thicknesses have been measured, as shown in Figure 6a. In addition, the absorption spectra of devices without top electrodes have been measured, as shown in Figure 6b. A small red shift in the spectra is seen as the PEDOT:PSS thickness is increased from 25 to 75 nm, along with the growth of the shoulder at 620 nm. Optical simulations have shown that these changes are not associated with interference effects.[25] The observed changes in spectra are consistent with an increase in the crystallinity of the P3HT

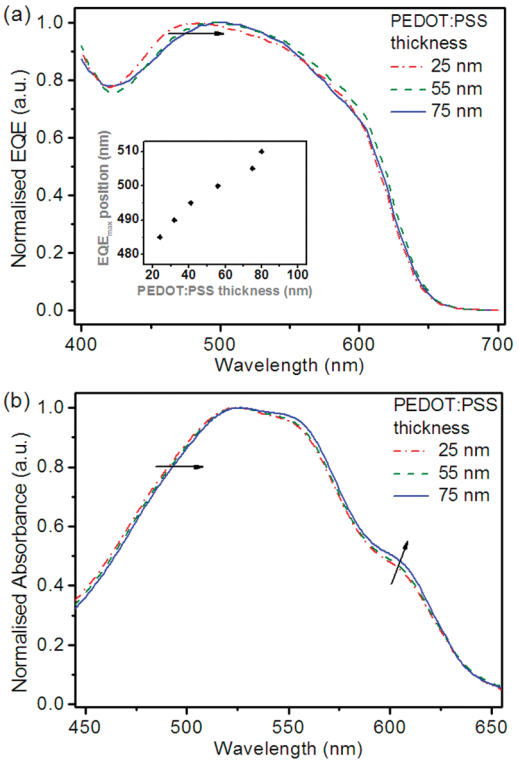

Figure 6. (a) EQE action spectra for devices with different PEDOT:PSS film thickness underneath the active layer, normalized to clarify change of shape and red shift upon increased film thickness. The inset shows the red shift of the EQE maximum with increasing PEDOT:PSS layer thickness. (b) Normalized absorbance of a F8TBT:P3HT blend on PEDOT:PSS-covered (25, 55, and 75 nm thickness) ITO−glass substrates.

component in the blend, which has previously been correlated with an improvement in device performance. Interestingly, the same shift does not occur for samples prepared on smooth quartz substrates, suggesting that smoothing of the ITO surface may be responsible for the improved crystallinity. Furthermore, we find that P3HT crystallinity is again reduced in samples deposited on PEDOT:PSS produced with very slow spin speeds, consistent with the enhanced roughness in those samples.

The changes in PEDOT:PSS surface roughness (and associated changes in active layer blend structure) discussed above provide a reasonable explanation for the changes in dark current and for the slight variations in EQE which are observed as the PEDOT:PSS thickness is altered. It is interesting to speculate on the cause of the changes observed in V_{oc} with PEDOT:PSS thickness. In principle, the maximum V_{oc} should be determined by the difference in energy between the donor HOMO level and acceptor LUMO level,[26,27] but the detailed electronic interaction of the active layer with the electrode can also play a role in setting V_{oc} in real devices. Changes in work function or density of states in the PEDOT:PSS electrode can therefore influence the measured V_{oc}. We also note that V_{oc} can be significantly affected by the blend structure in the immediate vicinity of the electrodes, particularly if there is a degree of surface segregation of one of the components.[28] The structure at the bottom electrode is likely to be highly sensitive to the chemical structure, surface energy, and roughness of the PEDOT:PSS surface, providing another possible cause for changes in V_{oc}.

2. Annealing Effects on PEDOT:PSS Films. *Photophysics and Device Performance.* The influence of annealing PEDOT:PSS

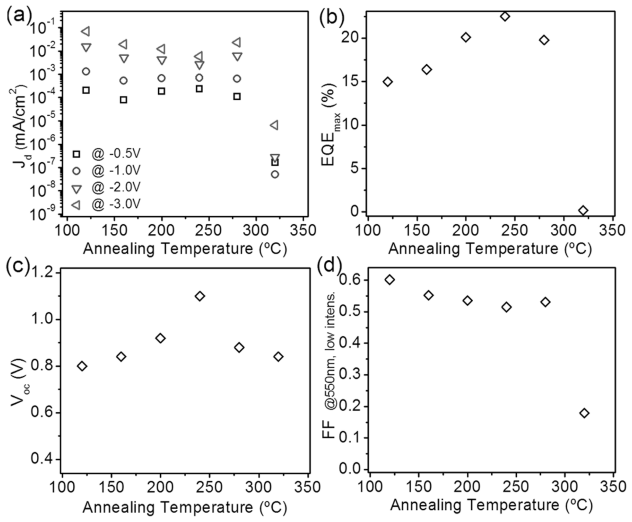

Figure 7. Photophysical characteristics of P3HT:F8TBT devices, dark current for various biases (a), EQE (b), open-circuit voltage (c), and fill factor (d) as a function of PEDOT:PSS annealing temperature.

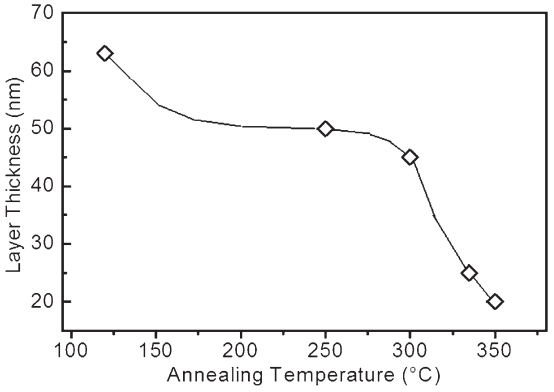

Figure 8. Film thickness as a function of PEDOT:PSS annealing temperature (line is drawn as a guide to the eye).

films on the performance of photovoltaic polymer blend devices with an active layer of F8TBT:P3HT has been studied, particularly focusing on dark current, external quantum efficiency, and current−voltage characteristics under illumination. PEDOT:PSS films were spun on ITO substrates, followed by annealing for 30 min under a nitrogen atmosphere at a temperature between 120 and 400 °C. Since annealing causes significant shrinkage in film thickness (as discussed later), it is necessary to adjust the spinning speed for different annealing temperatures to achieve a final thickness of 60 nm for all films after annealing, for comparability. The dependence of the dark current density on the PEDOT:PSS annealing temperature is shown in Figure 7a for different reverse bias values. A significant decrease of dark current density of more than 1 order of magnitude is observed when annealing temperature is raised from 120 to 240 °C, in particular at large reverse voltages. Further increase of annealing temperature to 280 °C increases the dark current again slightly. When an annealing temperature of 300 °C is exceeded, the dark current density of the final devices is decreased enormously, by about 3 orders of magnitude, indicating major structural changes in the PEDOT:PSS material. The maximum EQE values of these devices, which are displayed in Figure 7b, show a continuous increase with PEDOT:PSS annealing temperature from 120 to 250 °C. Annealing above 280 °C causes the EQE to drop slightly; further temperature increase above 300 °C reduces the

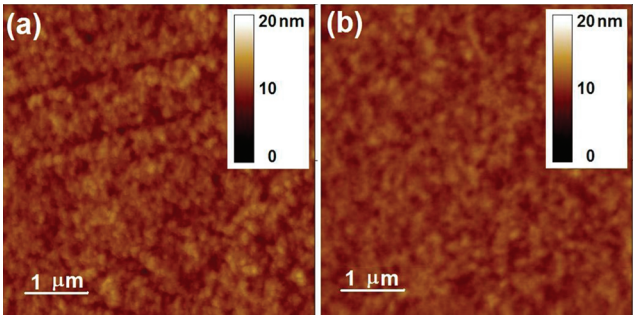

Figure 9. AFM topography images showing PEDOT:PSS films which have been annealed at (a) 120 °C and (b) 280 °C under a nitrogen atmosphere.

EQE drastically. The open-circuit voltage (Figure 7c) shows a particularly interesting dependence on annealing temperature, rising from 0.8 V for annealing at 120 °C to 1.2 V for annealing around 250 °C. Exceeding this temperature causes worsening, as previously observed for EQE and dark current, but the open-circuit voltage does not drop below 0.8 V, even for temperatures above 300 °C. The fill factor (Figure 7d) drops slightly with annealing at temperatures up to 300 °C and then drops rapidly. The significant changes seen in device performance with annealing merit further investigation of the physical changes occurring in the PEDOT:PSS films.

Morphological and Chemical Changes with Annealing. The first observation during annealing of PEDOT:PSS films spun under the same conditions is a considerable decrease of film thickness with rising temperature, as shown in Figure 8. During annealing from 120 up to 300 °C the thickness decreases by around 25%, presumably due to losses of water, primarily of interparticle liquid at lower temperature stages, followed by adsorbed and intraparticle liquid at higher temperatures. Further increase in temperature up to 350 °C reduces the thickness even more, with losses of around 75% of the initial thickness. This, together with the previous device results, strongly suggests that above 300 °C degradation of PEDOT:PSS takes place. AFM images of annealed PEDOT:PSS films, as shown for a 120 °C (Figure 9a) and a 280 °C (Figure 9b) sample, show also a reduction in particle/agglomerate size of PEDOT:PSS with increasing temperature, probably due to losses of water. This shrinkage is accompanied by reduced rms roughness, as would be expected.

To get a clearer image about temperature-dependent changes in PEDOT:PSS which could cause the differences in device performance and to clarify the nature of the material losses indicated by the thickness decrease, the material has been analyzed with a combination of TGA and FTIR. The TGA measurements (Figure 10a) quantify the material losses as a function of annealing temperature, whereas the infrared absorbance (Figure 10b) shows variations in the chemical structure on a molecular level. The TGA measurements, which have been performed on predried PEDOT:PSS material (prepared from colloidal solution by slow solvent evaporation at 90 °C, under flowing nitrogen), were carried out at a heating rate of 10 °C/min. Three very clear mass losses are obtained between 50 and 500 °C. The first one, ending around 150 °C, shows a mass loss of about 17%, which is quite consistent with the reduced film thickness of about 19%. A second loss of around 38% appears between 220 and 320 °C. A final mass loss of more than 30% occurs between 350 and 450 °C. While the first mass loss can clearly be ascribed to losses of water, the next two losses are more difficult to identify and hence are

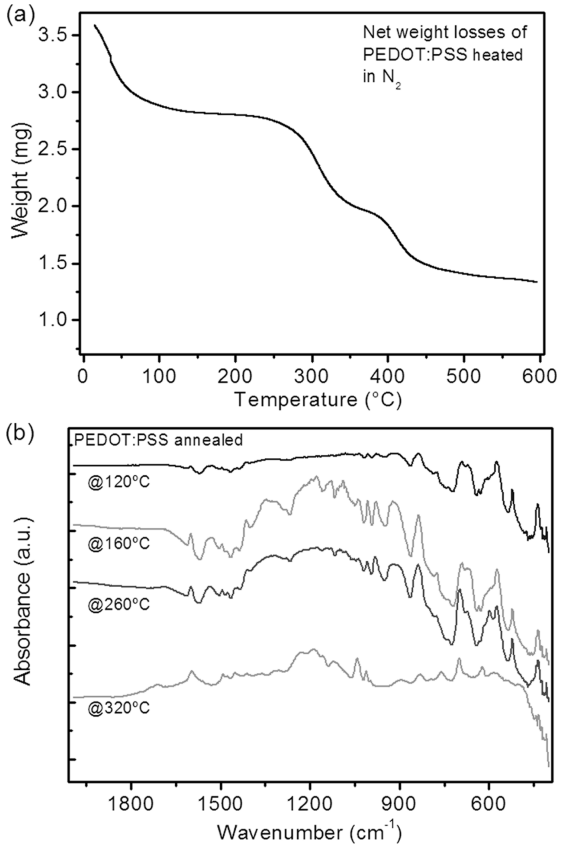

Figure 10. (a) TGA measurement on PEDOT:PSS under a nitrogen atmosphere, with a heating rate of 10 °C/min. (b) IR absorption of annealed PEDOT:PSS films, offset for clarity.

investigated in more detail by FTIR. Since PEDOT and PSS show partially superposed vibrations, the assignment of a specific absorption band is not always clear. In particular, the thiophene and phenyl rings in PEDOT and PSS, respectively, have vibrations between 1350 and 1600 cm^{-1} and hence are hard to distinguish. Therefore, in the literature the vibrations of the ethylenedioxy group, specifically the C−O−C stretching modes at around 1070 and 1240 cm^{-1}, are typically used to identify PEDOT.[29,30] For PSS the sulfonic acid is usually used for identification,[31−34] particularly the vibrations below 600 cm^{-1}, the S=O vibration at 1180 cm^{-1}, and the O−S−O signal at 1030 cm^{-1}. All these characteristic absorptions can be found in the measured FTIR spectra in Figure 10b, for the samples annealed up to 260 °C. Apart from slightly smeared absorptions in the 120 °C sample (probably due to too much remaining adsorbed water), the spectra do not show significant changes due to annealing, indicating that the chemical structure of the PEDOT:PSS part stays intact up to quite high temperatures, including 250 °C, which represents the temperature for optimum device performance. Above this temperature, and especially above 300 °C, chemical changes become obvious. The major changes seen are the disappearance of the sulfonic acid vibrations below 600 cm^{-1} and of an unassigned peak at 1542 cm^{-1}. The region between 1530 and 1560 cm^{-1} is known to contain absorptions due to aromatic ring deformation vibrations, and the position and strength of these features are strongly dependent on the substituent attached to the ring. It is therefore likely that 1542 cm^{-1} absorption is due to the deformation of phenyl rings with attached sulfonate groups.[35,36] Hence, we can infer from FTIR spectra that, during annealing of PEDOT:PSS at

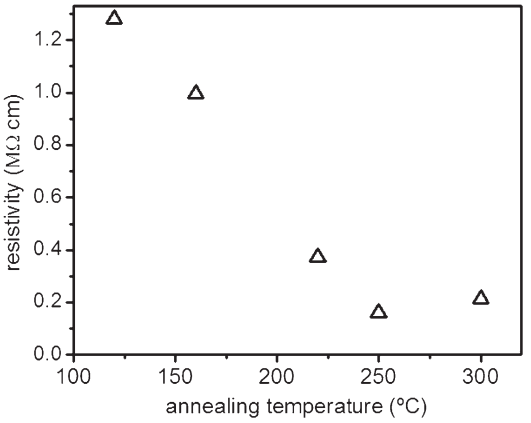

Figure 11. Resistivity of PEDOT:PSS films as a function of annealing temperature.

temperatures above 260 °C, the PSS degrades via rupture of the sulfonate group from styrene, which could explain the second weight loss step in the TGA results. This agrees well with literature reports of outgassing of SO_2/SO_3 from PSS heated to temperatures around 250 °C.[37] On the basis of the known PEDOT:PSS ratio of 1:16, a mass loss of 41% is expected for complete scission of sulfonic acid, consistent with the measured weight loss of 38%. We have not investigated in detail the chemical changes associated with the third mass loss, from 350 °C onward, but this is likely to be associated with rupture of the polymer backbones.[38,39] No phase transitions of PEDOT:PSS, such as crystallization or melting, could be detected upon annealing up to 400 °C (with DSC or DMA).

To investigate changes in PEDOT:PSS conductivity, two-point-probe measurements have been performed on PEDOT:PSS films, annealed between 120 and 300 °C, measured in-plane across a 40 μm channel (Figure 11). Films annealed up to 250 °C show a continuous decrease in resistivity, with only a slight further increase seen at higher temperatures. The changes seen at temperatures up to 160 °C may be associated with the evaporation of water, leading to shrinkage of the insulating PSS shell surrounding the conducting PEDOT-rich grains. Above that temperature, PSS segregation effects, as reported in literature, may improve conductivity.[10,14,40] At temperatures exceeding 250 °C the falling conductivity is probably caused by the onset of PSS degradation.

The improvement seen in device performance with annealing at temperatures up to 250 °C occurs in a region when there are no major chemical changes in the PEDOT:PSS itself, only a loss of water and probably structural changes such as segregation. Above 300 °C the device performance falls off rapidly, but we find that this change is not simply due to degradation in the PEDOT:PSS bulk conductivity. Instead, it is likely to be due to changes in surface properties (e.g., work function), which are sensitive to removal of sulfonic acid.

Conclusions

In this work, the influence of PEDOT:PSS film thickness and annealing procedures on the performance of polymer−polymer photovoltaic devices has been investigated. We find that there is an optimum thickness, of 70 nm, for the PEDOT:PSS layer, and that this is independent of the overlying active material. Changes in surface roughness are found to be largely responsible for this effect. Annealing of the PEDOT:PSS prior to deposition of the active layer is found to have a significant effect on device

performance, with an optimum at 250 °C. The improvement with annealing can be mainly explained by losses of inter- and intraparticle water. Above this temperature degradation of the PSS is found to occur by loss of sulfonic acid groups, leading to a breakdown in device performance.

Acknowledgment. We are grateful to Cambridge Display Technology Ltd. (CDT) for the supply of materials, to the Technology Strategy Board for funding, as part of the OPALS (TP/K2512F) collaborative project with CDT and Molecular Vision Ltd., and to Dr. J. J. M. Halls and Dr. A. B. Doust for useful discussions.

References and Notes

(1) Groenendaal, L.; Jonas, F.; Freitag, D.; Pielartzik, H.; Reynolds, J. R. *Adv. Mater.* **2000**, *12*, 481–494.
(2) Nardes, A. M.; Kemerink, M.; de Kok, M.; Vinken, E.; Maturova, K.; Janssen, R. A. J. *Org. Electron.* **2008**, *9*, 727–734.
(3) Jonas, F.; Heywang, G. *Electrochim. Acta* **1994**, *39*, 1345–1347.
(4) Jönsson, S. K. M.; Birgerson, J.; Crispin, X.; Greczynski, G.; Osikowicz, W.; Denier van der Gon, A. W.; Salaneck, W. R.; Fahlman, M. *Synth. Met.* **2003**, *139*, 1–10.
(5) Hwang, J.; Amy, F.; Kahn, A. *Org. Electron.* **2006**, *7*, 387–396.
(6) Kirchmeyer, S.; Reuter, K. *J. Mater. Chem.* **2005**, *15*, 2077–2088.
(7) Crispin, X.; Marciniak, S.; Osikowicz, W.; Zotti, G.; Denier van der Gon, A. W.; Louwet, F.; Fahlman, M.; Groenendaal, L.; De Schryver, F.; Salaneck, W. R. *J. Polym. Sci., Part B: Polym. Phys.* **2003**, *41*, 2561–2583.
(8) Greczynski, G.; Kugler, T.; Keil, M.; Osikowicz, W.; Fahlman, M.; Salaneck, W. R. *J. Electron Spectrosc. Relat. Phenom.* **2001**, *121*, 1–17.
(9) Nardes, A. M.; Kemerink, M.; Janssen, R. A. J.; Bastiaansen, J. A. M.; Kiggen, N. M. M.; Langeveld, B. M. W.; van Breemen, A. J. J. M.; de Kok, M. M. *Adv. Mater.* **2007**, *19*, 1196–1200.
(10) Pingree, L. S. C.; MacLeod, B. A.; Ginger, D. S. *J. Phys. Chem. C* **2008**, *112*, 7922–7927.
(11) (a) Fan, B.; Mei, X.; Ouyang, J. *Macromolecules* **2008**, *41*, 5971–5973. (b) Huang, J.; Miller, P. F.; Wilson, J. S.; de Mello, A. J.; de Mello, J. C.; Bradley, D. D. C. *Adv. Funct. Mater.* **2005**, *15*, 290–296.
(12) Kim, W. H.; Kushto, G. P.; Kim, H.; Kafafi, Z. H. *J. Polym. Sci., Part B: Polym. Phys.* **2003**, *41*, 2522–2528.
(13) Yang, X. H.; Jaiser, F.; Stiller, B.; Neher, D.; Galbrecht, F.; Scherf, U. *Adv. Funct. Mater.* **2006**, *16*, 2156–2162.
(14) Kim, Y.; Shin, M.; Kim, H. *Macromol. Res.* **2008**, *16*, 185–188.
(15) Aasmundtveit, K. E.; Samuelsen, E. J.; Pettersson, L. A. A.; Inganas, O.; Johansson, T.; Feidenhans'l, R. *Synth. Met.* **1999**, *101*, 561–564.
(16) Kim, Y.; Ballantyne, A. M.; Nelson, J.; Bradley, D. D. C. *Org. Electron.* **2009**, *10*, 205–209.
(17) Nguyen, T. P.; Le Rendu, P.; Long, P. D.; De Vos, S. A. *Surf. Coat. Technol.* **2004**, *180−181*, 646–649.
(18) Vitoratos, E.; Sakkopoulos, S.; Dalas, E.; Paliatsas, N.; Karageorgopoulos, D.; Petraki, F.; Kennou, S.; Choulis, S. A. *Org. Electron.* **2009**, *10*, 61–66.
(19) Friedel, B.; Brenner, T. J. K.; McNeill, C. R.; Greenham, N. C., to be published.
(20) Keivanidis, P. E.; Howard, I. A.; Friend, R. H. *Adv. Funct. Mater.* **2008**, *18*, 3189–3202.
(21) Keivanidis, P. E.; Greenham, N. C.; Sirringhaus, H.; Friend, R. H.; Blakesley, J. C.; Speller, R.; Agostinelli, T.; Campoy-Quiles, M.; Bradley, D. D. C.; Nelson, J. *Appl. Phys. Lett.* **2008**, *92*, 023304.
(22) McNeill, C. R.; Halls, J. J. M.; Wilson, R.; Whiting, G. L.; Berkebile, S.; Ramsey, M. G.; Friend, R. H.; Greenham, N. C. *Adv. Funct. Mater.* **2008**, *18*, 2309–2321.
(23) Li, Q.; Jonas, U.; Zhao, X. S.; Kappl, M. *Asia-Pac. J. Chem. Eng.* **2008**, *3*, 255–268.
(24) Kralchevsky, P. A.; Denkov, N. D. *Curr. Opin. Colloid Interface Sci.* **2001**, *6*, 383–401.
(25) Persson, N.-K.; Arwin, H.; Inganas, O. *J. Appl. Phys.* **2005**, *97*, 034503.
(26) Mihailetchi, V. D.; Blom, P. W. M.; Hummelen, J. C.; Rispens, M. T. *J. Appl. Phys.* **2003**, *94*, 6849–6854.
(27) Brabec, C. J.; Cravino, A.; Meissner, D.; Sariciftci, N. S.; Fromherz, T.; Rispens, M. T.; Sanchez, L.; Hummelen, J. C. *Adv. Funct. Mater.* **2005**, *11*, 374–380.
(28) Khodabakhsh, S.; Sanderson, B. M.; Nelson, J.; Jones, T. S. *Adv. Funct. Mater.* **2006**, *16*, 95–100.
(29) Han, M. G.; Foulger, S. H. *Adv. Mater.* **2004**, *16*, 231–234.
(30) Kvarnström, C.; Neugebauer, H.; Blomquist, S.; Ahonen, H. J.; Kankare, J.; Ivaska, A. *Electrochim. Acta* **1999**, *44*, 2739–2750.
(31) Cristovan, F. H.; Nascimento, C. M.; Bell, M. J. V.; Laureto, E.; Duarte, J. L.; Dias, I. F. L.; Cruz, W. O.; Marletta, A. *Chem. Phys.* **2006**, *326*, 514–520.
(32) Neelgund, G. M.; Hrehorova, E.; Joyce, M.; Bliznyuk, V. *Polym. Int.* **2008**, *57*, 1083–1089.
(33) Martins, C. R.; de Freitas, P. S.; De Paoli, M.-A. *Polym. Bull.* **2003**, *49*, 379–386.
(34) Sun, B.; Zhao, Y.; Wu, J. G.; Yang, Q.-C.; Xu, G.-X. *J. Mol. Struct.* **1998**, *470*, 63–66.
(35) Chen, A. C.; Sun, S. G.; Yang, D. F.; Pettinger, B.; Lipkowski, J. *Can. J. Chem.* **1996**, *74*, 2321–2330.
(36) Sheng, C.; Wenting, B.; Shijian, T.; Yuechuan, W. *J. Appl. Polym. Sci.* **2008**, *109*, 120–125.
(37) Greczynski, G.; Kugler, T.; Salaneck, W. R. *Thin Solid Films* **1999**, *354*, 129–135.
(38) Wilson, K.; Lee, A. F.; Macquarrie, D. J.; Clarc, J. H. *Appl. Catal., A* **2002**, *228*, 127–133.
(39) Kiebooms, R.; Aleshin, A.; Hutchison, K.; Wudl, F.; Heeger, A. *Synth. Met.* **1999**, *101*, 436–437.
(40) Kemerink, M.; Timpanaro, S.; de Kok, M. M.; Meilenkamp, E. A.; Touwslager, F. J. *J. Phys. Chem. B* **2004**, *108*, 18820–18825.